INSTITUTE OF PHYSICS PUBLISHING NONLINEARITY

Nonlinearity **15** (2002) 25–43 PII: S0951-7715(02)23553-7

Periodic orbit theory applied to a chaotically oscillating gas bubble in water

G Simon[1], P Cvitanović[2], M T Levinsen[3], I Csabai[4] and Á Horváth[1]

[1] Department of Atomic Physics, Eötvös Loránd University, H-1117 Budapest, Hungary
[2] Center for Nonlinear Science, School of Physics, Georgia Institute of Technology, Atlanta, GA 30332-0430, USA
[3] Center for Chaos and Turbulence Studies, Niels Bohr Institute, Blegdamsvej 17 DK 2100, Copenhagen Ø, Denmark
[4] Department of Physics of Complex Systems, Eötvös Loránd University, H-1117 Budapest, Hungary

Received 3 April 2001, in final form 17 August 2001
Published 26 November 2001
Online at stacks.iop.org/Non/15/25

Recommended by J P Keating

Abstract

This study investigates the dynamics of an acoustically driven air bubble in water. Depending on the values of external parameters, the radial oscillations of the bubble can be either stable or chaotic. The necessary condition of chaotic behaviour is identified to be the non-zero amplitude of the bubble's afterbounces at the beginning of the next acoustic cycle, which brings memory into the system. We show that for some parameter values in the chaotic regime the dynamics can be reduced to a unimodal map. At these parameter values the periodic orbit theory is successfully applied to calculate averages of relevant physical quantities, such as the air concentration at which the bubble is in diffusive equilibrium with the surrounding liquid. Finally we investigate the convergence of the calculated quantities.

Mathematics Subject Classification: 37C27, 37B10, 76B10

1. Introduction

A gas bubble levitated in a liquid by ultrasound is the subject of recent experimental and theoretical studies in the field of single-bubble sonoluminescence (SBSL) [1–3]. At sufficiently high amplitudes of the acoustic excitation the non-linear oscillations of the bubble can get so violent, that in each period the bubble collapses to its van der Waals hard core radius. As a result the gas inside the bubble compresses and heats up to the extent that light emission occurs [4–9] while the bubble is at its minimum radius. In one of the first experiments with single bubbles, Barber *et al* [10] found a remarkably stable dynamics, a synchronicity

with the driving sound field (typically ≈27 kHz) on the order of 50 ps. Later Holt *et al* [11] also reported period doubling, quasiperiodicity and chaos in the timing of successive flashes and Jensen [12] observed period doubling in the light emission, but the underlying mechanism responsible for the observed behaviour has not yet been identified. Previous studies by Lauterborn and Suchla [13] investigated a particular bubble dynamical model in the context of acoustic cavitation [14] and showed that the radial oscillations of a gas bubble can undergo period-doubling bifurcations and become chaotic. Related theoretical works can also be found in [15–17], and references therein. It was proposed in [11] that the same mechanism could explain the observed period-doubling and chaotic behaviour in the SBSL measurements; however the parameter space that was studied previously is far from that which is relevant for SBSL or the studied models were oversimplified by the assumptions of ideal gas law, absence of heat transfer, and negligence of surface tension effects. One of our aims is to elucidate this question by performing extensive numerical simulations in a wide range of the parameters. The main purpose of this study however is to show how periodic orbit theory can be used to calculate the averages of physical quantities of interest for the case of chaotic radial oscillations.

2. The Rayleigh–Plesset equation

The equation of motion of the interface radius $R(t)$ for a spherically oscillating gas bubble under harmonic excitation is given by the Rayleigh–Plesset (RP) equation [18–20]. We consider a particular form of the RP equation which has been investigated in recent theoretical and experimental studies, namely

$$\rho_{\mathrm{w}}\left(R\ddot{R}+\frac{3}{2}\dot{R}^2\right)=P_{\mathrm{g}}(R(t))-P_{\mathrm{f}}(t)-P_0+\frac{R}{c_{\mathrm{w}}}\frac{\mathrm{d}}{\mathrm{d}t}[P_{\mathrm{g}}(R(t))-P_{\mathrm{f}}(t)]-4\eta\frac{\dot{R}}{R}-\frac{2\sigma}{R}, \quad (1)$$

where the left-hand side is the inertial term, and the terms on the right-hand side give the various pressures acting on the interface. In particular $P_0 = 1$ bar is the static ambient pressure, $P_{\mathrm{f}} = -P_{\mathrm{a}}\sin(\omega t)$ is the forcing pressure with angular frequency ω and acoustic pressure amplitude P_{a}, and P_{g} is the uniform gas pressure inside the bubble, given by a van der Waals equation of state,

$$P_{\mathrm{g}}(R(t))=\left(P_0+\frac{2\sigma}{R_0}\right)\frac{(R_0^3-a^3)^\gamma}{(R(t)^3-a^3)^\gamma}, \quad (2)$$

where R_0 is the ambient radius (stationary radius under normal temperature and pressure), $a = R_0/8.5$ is the hard core van der Waals radius for air, and γ is the polytropic exponent, which is 1 for an isothermic process, and greater than 1 for an adiabatic process, where the actual value depends on the choice of the gas. It must be noted that the assumption of uniformity is an approximation, but its validity is justified in most of the acoustic cycle [21]. The material constants of water appearing in the RP equation are given in table 1. In order to solve the RP equation numerically, it was transformed into the following set of first-order differential

Table 1. Notation and room temperature values of material constants in equation (1).

Density	ρ_{w}	1000	$\mathrm{kg\,m^{-3}}$
Velocity of sound	c_{w}	1481	$\mathrm{m\,s^{-1}}$
Dynamic viscosity	η	1×10^{-3}	$\mathrm{kg\,m^{-1}\,s^{-1}}$
Surface tension	σ	0.073	$\mathrm{N\,m^{-1}}$

equations:

$$\dot{R} = V,$$
$$\dot{V} = \frac{1}{\rho_w R}(P_g - P_f - P_0 - P_\eta - P_\sigma + P_s) - \frac{3}{2R}V^2, \tag{3}$$

where the pressure terms are defined as

$$P_f = -P_a \sin(\omega t), \qquad P_\eta = \frac{4\eta V}{R}, \qquad P_\sigma = \frac{2\sigma}{R}, \qquad P_s = \frac{R}{c_w}\frac{d}{dt}(P_g - P_f). \tag{4}$$

As a general remark it can be noted that the set of equations (3) describes a highly non-linear, non-autonomous dynamical system in a two-dimensional phase space.

The adjustable parameters that were varied during the simulations are the amplitude of the forcing P_a and the ambient radius R_0, while the angular frequency ω was kept at the constant value of $\omega = 2\pi \cdot 27\,\text{kHz}$ used in the experiment of Holt *et al* [11]. The numerical simulations were performed by a fifth-order Runge–Kutta algorithm with adaptive stepsize control [22]. If not otherwise mentioned, all the simulations used $\gamma = 5/3$, initial values of $R(t = 0) = R_0$, $V(t = 0) = 0$, and the values of the material constants from table 1.

3. Stability and chaos

Before the detailed investigation of the dynamics can take place, first we need to find the regions in the (P_a, R_0) parameter space, where the solutions of the RP equation are stable or exhibit chaos. For this purpose equations (3) were solved for 100 acoustic periods in a wide range of P_a and R_0 and the values of the maximal radii R_{max} were extracted for each pair of the parameters. The condition

$$\left| \frac{R_{max}^{(N-1)} - R_{max}^{(N)}}{R_{max}^{(N-1)}} \right| \geqslant \alpha_{tr} \tag{5}$$

was used to identify parameter space points where the variations of R_{max} after N cycles still stayed above a chosen small threshold value α_{tr}. Figure 1 shows the results for (*a*) $N = 5$, (*b*) $N = 100$ with $\alpha_{tr} = 0.001$. It is apparent from these figures that non-steady radial oscillations can be expected only for big enough bubbles ($R_0 \geqslant 7\,\mu\text{m}$) at rather high forcing

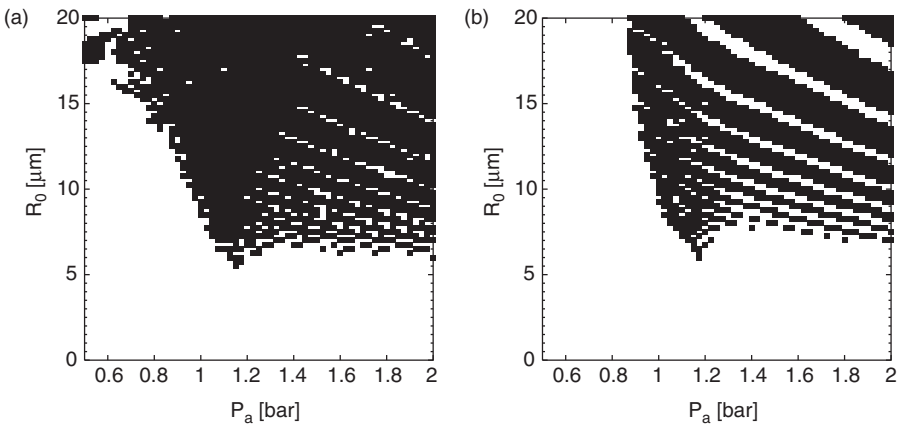

Figure 1. Parameter space points (black region), where condition (5) is fulfilled for $N = 5$ (*a*), $N = 100$ (*b*) and $\alpha_{tr} = 0.001$.

($P_a \geqslant 0.8$ bar), while in the whole parameter space of SBSL, which is restricted by shape instability thresholds to $R_0 \leqslant 6$–$7\,\mu$m [23–28] (for this acoustic frequency), the dynamics is stable. This observation suggests that the period-doubling and chaotic behaviour observed in the measurements of Holt *et al* did not originate from pure RP dynamics. Nevertheless it is still interesting to investigate the chaotic behaviour of the RP equation since it can be relevant in the field of acoustic cavitation [14] or multibubble sonoluminescence. For instance, [29] reports transient cavitation measurements at parameter values ($\omega \approx 11$ MHz, $P_a \approx 100$ bar, $R_0 \approx 0.5\,\mu$m), where the solutions to the RP equation show period-doubled and chaotic behaviour.

In order to better understand the mechanism which leads to chaos in the particular system, it is useful to compare the characteristics of the stable and chaotic solutions to the RP equation. Figure 2 shows a stable solution over one acoustic period, at parameter values ($P_a = 1.36$ bar, $R_0 = 3\,\mu$m, and $\omega/2\pi = 27$ kHz) typical in SBSL experiments.

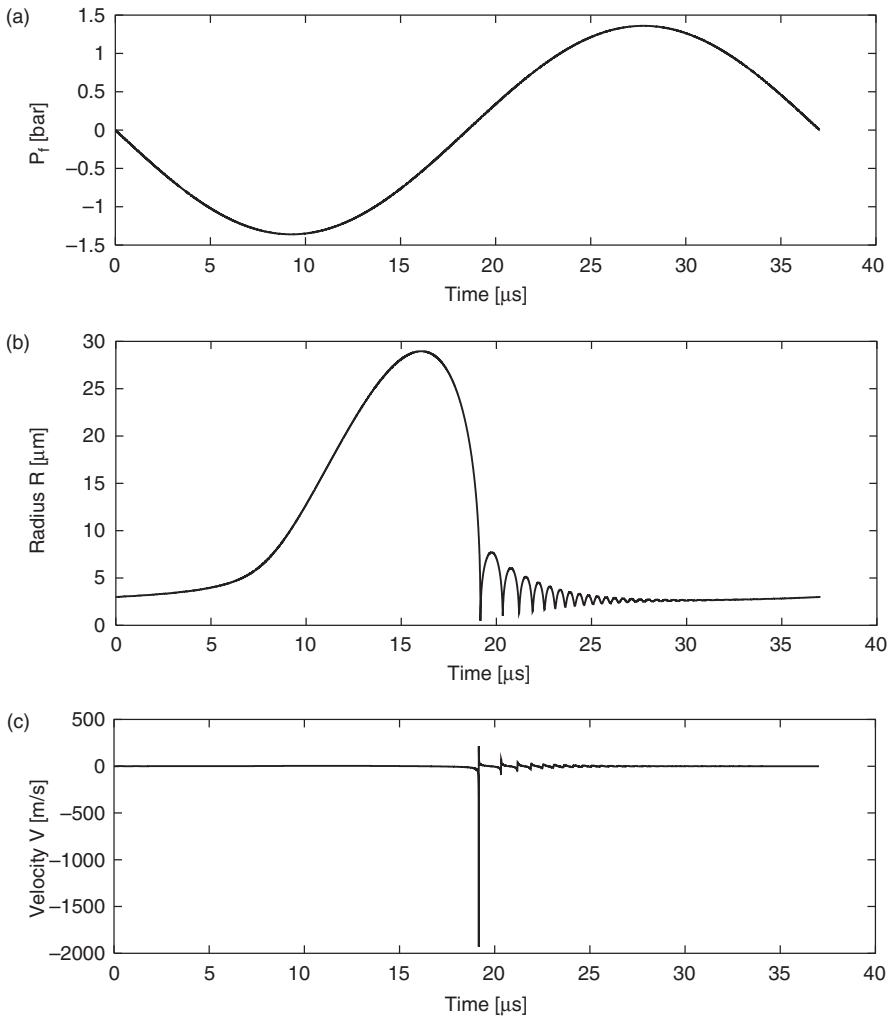

Figure 2. The driving pressure (*a*), the radius of the bubble (*b*), and the velocity of its interface (*c*) as a function of time for one acoustic cycle. The parameters are $P_a = 1.36$ bar, $R_0 = 3\,\mu$m, $\gamma = 5/3$, and $\omega/2\pi = 27$ kHz.

The non-linear oscillations of such bubbles are characterized by a big variety of spatial and temporal scales. Initially the radius is at its ambient value R_0. Then during the negative part of the sinusoidal driving the bubble slowly ($t_{\mathrm{exp}} \approx 1/2T_p$) expands to its maximum ($\approx 10R_0$). At this instant the pressure inside the bubble approaches vacuum. The increasing driving pressure then makes the bubble collapse. The time to go from R_0 to the minimum radius is approximately given by [3]

$$t_{\mathrm{c}} \approx \frac{\sqrt{6}R_0^{5/2}}{5R_{\mathrm{max}}^{3/2}(P_0/\rho_{\mathrm{w}})^{1/2}}. \tag{6}$$

For high forcing amplitudes the bubble at minimum reaches its hard core van der Waals radius ($R_0/8.5$), which results in enormous pressures and temperatures inside it (order of magnitudes: 10^4 bar and 10^4 K) and also in a flash of light. In the late stages of the collapse the interface velocity can be even higher than the speed of sound in the liquid which results in an outgoing shock wave in the water [30–32]. The main collapse is followed by a sequence of afterbounces with decreasing amplitude, after which the whole process repeats itself in the next acoustic cycle. The angular frequency of the afterbounces is approximately

$$\omega_{\mathrm{b}} \approx \sqrt{\frac{1}{\rho_{\mathrm{w}}R_0^2}\left(3\gamma\left(P_0 + \frac{2\sigma}{R_0}\right) - \frac{2\sigma}{R_0} - \frac{4\eta^2}{\rho_{\mathrm{w}}R_0^2}\right)} \tag{7}$$

(see for instance [12]). An important feature of figure 2, which is also the reason for the stability of the cycle, is that the amplitude of the afterbounces dies away completely before the beginning of the next cycle and thus the radius and the interface velocity at the end of the cycle equal the initial values.

If the ambient radius is increased to $R_0 = 20\,\mu\mathrm{m}$, the solution to the RP equation shifts to the chaotic regime. Figure 3 shows the oscillations of such a bubble over eight acoustic

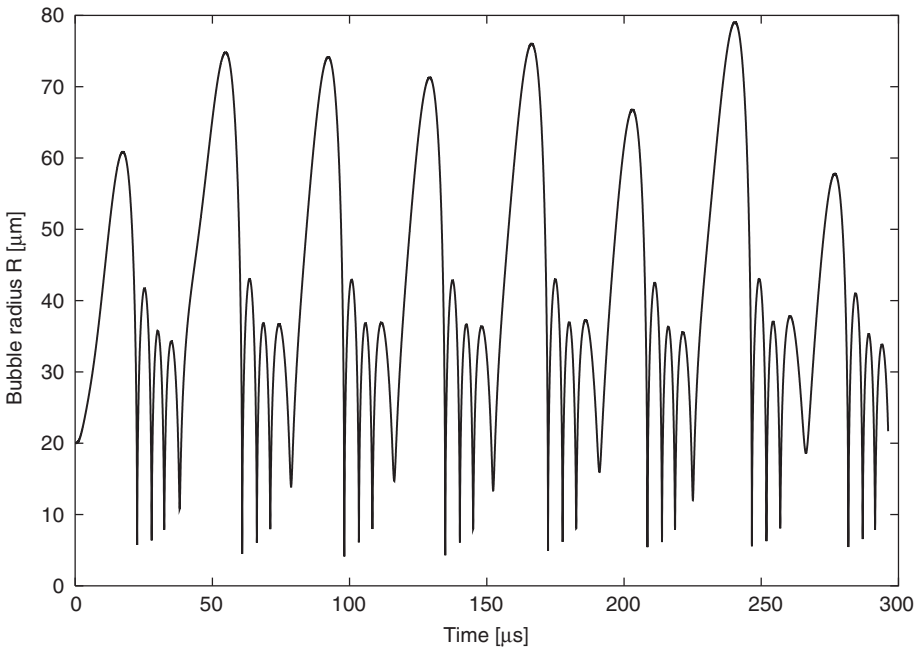

Figure 3. Radius of the bubble over eight acoustic cycles. The parameters are $P_{\mathrm{a}} = 1.26\,\mathrm{bar}$, $R_0 = 20\,\mu\mathrm{m}$, $\gamma = 5/3$, and $\omega/2\pi = 27\,\mathrm{kHz}$.

periods. This regime differs from the stable solution in several aspects. Probably the most important aspect is that due to the increased R_0 the angular frequency of the afterbounces is decreased. As a result there is not enough time for the afterbounces to be damped out completely before the next expansion begins. Thus each new acoustic cycle will have the 'memory' of the undamped amplitude from the previous cycle, resulting in big variations in the maximal radii. In particular, the $\omega_b \approx 7 \times \omega$ in figure 3 is in good agreement with equation (7). The attractor in the phase space (R, V) for $P_a = 1.255$ bar is shown in figure 4. A magnification of the attractor around the maximal radius shows that the trajectory fills up the phase space between 60 and 80 μm.

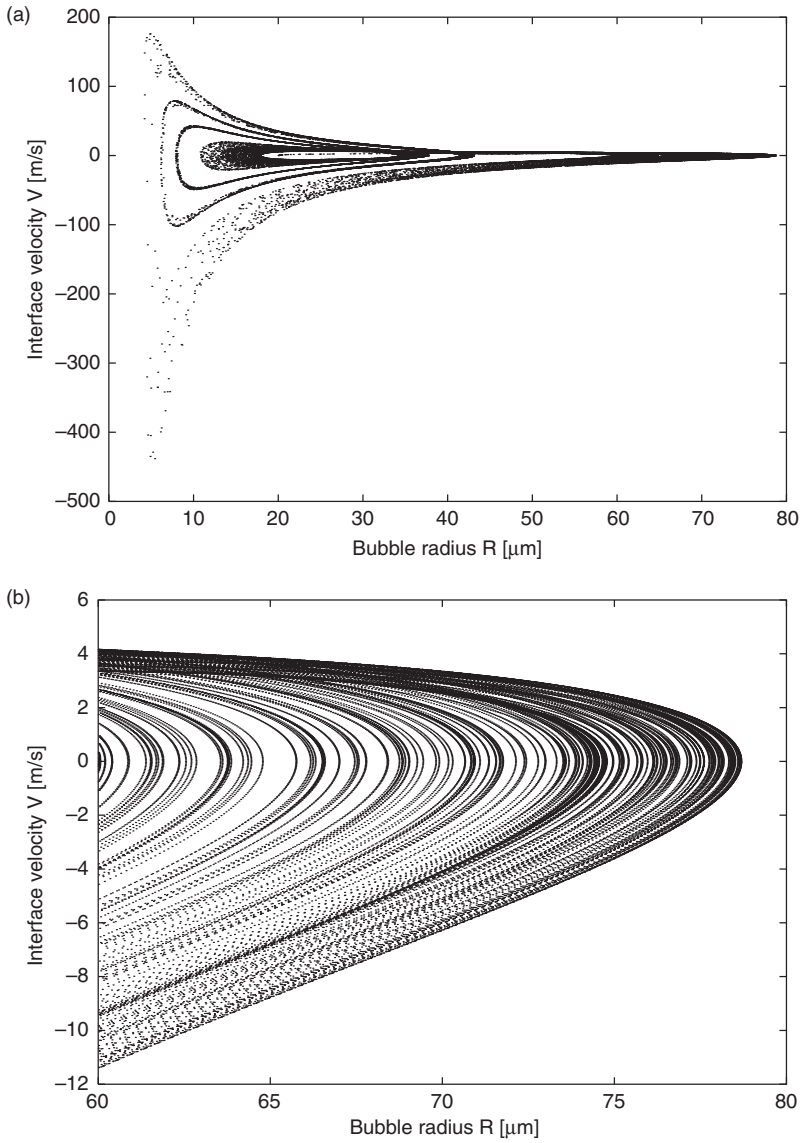

Figure 4. The chaotic attractor (*a*) and a region blown up around the maximal radius (*b*) for 100 cycles. The parameters are $P_a = 1.255$ bar, $R_0 = 20\,\mu$m, $\gamma = 5/3$, and $\omega/2\pi = 27$ kHz.

After chaos is found at a particular point in the parameter space (P_a, R_0, $\omega/2\pi$), it is interesting to investigate how the system behaves upon changing these parameters. Since mapping out numerically the whole parameter space is very time consuming, only the effect of changing the driving amplitude P_a is presented here. Such an analysis is usually carried out in a Poincaré section (P) of the phase space, since it describes the dynamics just as well (by constructing a Poincaré map), and allows one to draw the parametric dependence in a plane. The choice of Poincaré section is arbitrary; the only necessary condition is that the trajectory should cross the plane of the section once every acoustic cycle. For driven systems one choice can be to get samples from a given part of each driving period. However a more general method, namely to set one of the phase space coordinates to zero, can also be applied. For this study the condition

$$P \equiv \max_R \{(R, V) : V = 0\} \tag{8}$$

was used, which gives the maximal radii from each acoustic period. Figure 5 shows the results for $R_0 = 20\,\mu\text{m}$, $\gamma = 5/3$, and $\omega/2\pi = 27\,\text{kHz}$. At each value of P_a the RP equation was solved for 500 cycles, and a Poincaré section was constructed by applying (8). Out of 500 cycles only the last 200 are shown in the figure, thus cutting out the uninteresting initial transients. For small enough forcing ($P_a \leqslant 0.85\,\text{bar}$) the dynamics is regular. Then a jump occurs, and the solution becomes chaotic after a period-doubling bifurcation sequence, showing the same qualitative features as reported in [13]. Inside the chaotic region one can observe windows of regular dynamics, stable three-period solutions, and so on, just as for the well-known logistic map. Figure 6 shows the return maps at different driving levels covering dynamics with (*a*) two-period, (*b*) four-period, chaos, and (*f*) inside the chaotic region a three-period regime.

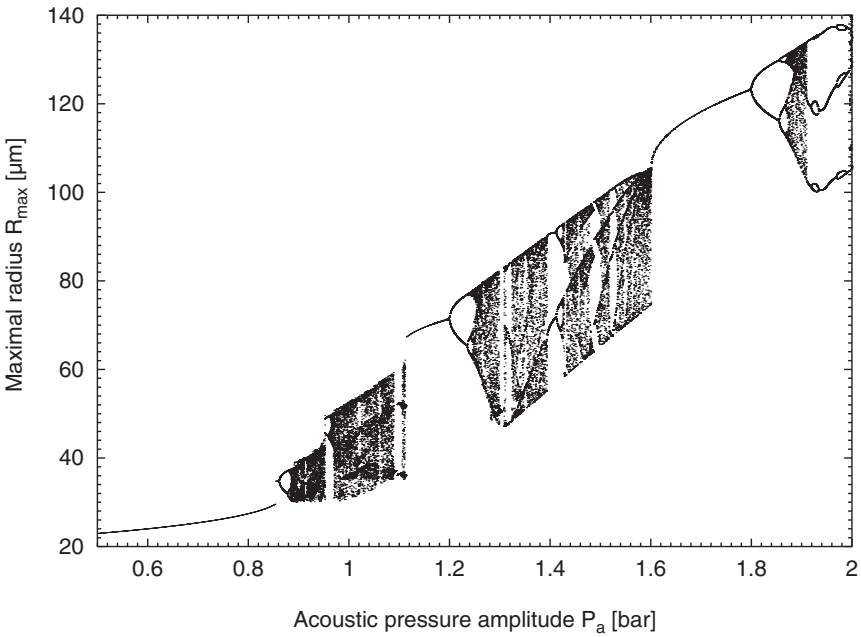

Figure 5. Bifurcation diagram of the maximal radius for $R_0 = 20\,\mu\text{m}$, $\gamma = 5/3$, and $\omega/2\pi = 27\,\text{kHz}$.

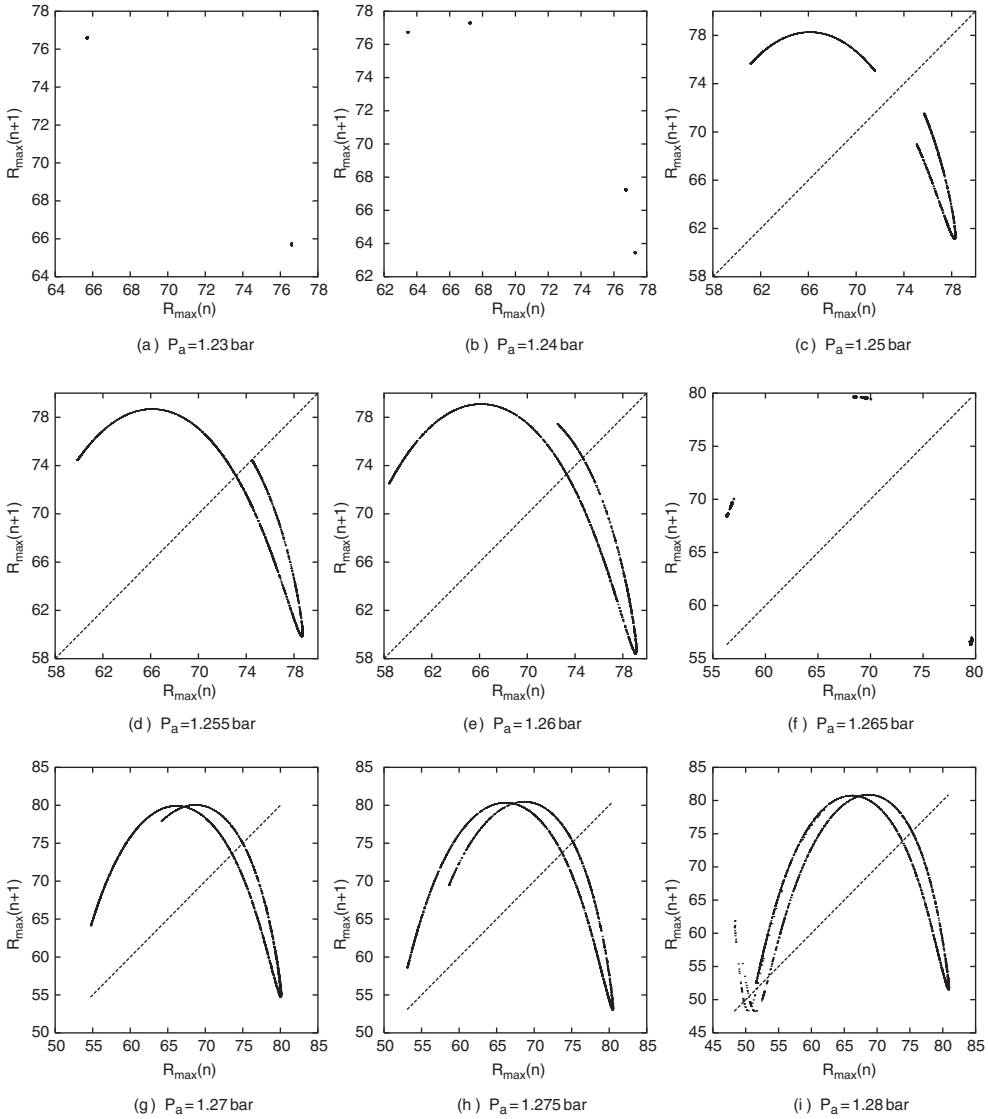

Figure 6. Return maps of maximal radii at different values of P_a. The other parameters are $R_0 = 20\,\mu\text{m}$, $\gamma = 5/3$, and $\omega/2\pi = 27\,\text{kHz}$.

Note the non-uniqueness and the increased complexity of the return maps with increased driving amplitude. Qualitatively the same kind of maps have been observed if the transition from regular dynamics to chaos is examined at driving levels around 0.88 and 0.96 bar.

In figure 7 another observable ξ is shown as a function of the driving level. It gives the phase of the minimal radius in the acoustic period, and is defined as $\xi = t/T$, where t is the elapsed time from the beginning of the cycle until the radius reached its minimum, and T is the acoustic period. This elapsed time offers a better comparison between simulation and experimental data obtained for instance by the Mie scattering technique [33, 34] (the timing of the scattered light at the collapses can be measured with higher precision than its

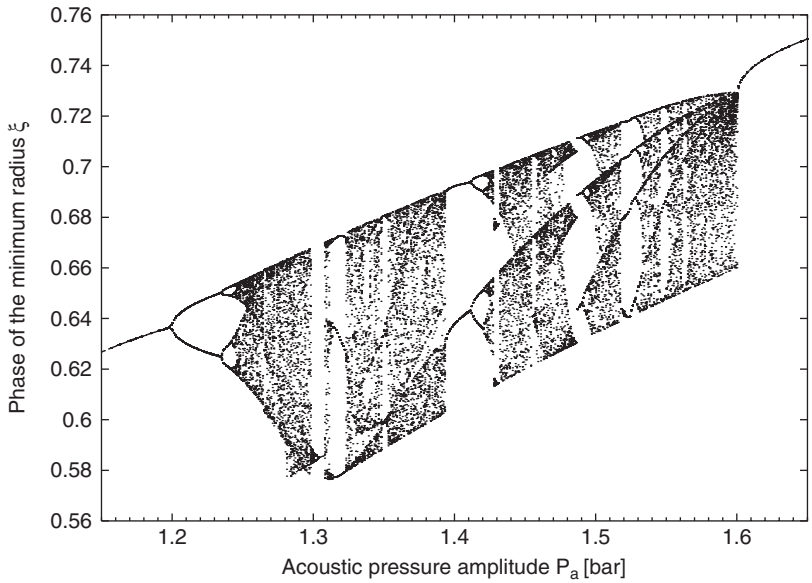

Figure 7. Bifurcation diagram of ξ for $R_0 = 20\,\mu\text{m}$, $\gamma = 5/3$, and $\omega/2\pi = 27\,\text{kHz}$.

amplitude). Also ξ is the key observable of a fitting technique [35] that can be used to obtain the parameters of the bubble dynamics in measurements. The bifurcation diagram for ξ shows the same qualitative features as the one obtained for the maximal radii. This is however not surprising, since the topology of the bifurcation diagrams should not depend on the particular choice of the Poincaré section, and the values of ξ were extracted from the minimal radii, which by the condition

$$P \equiv \min_R \{(R, V) : V = 0\} \tag{9}$$

also define a Poincaré section.

Although conditions (8) and (9) are convenient for drawing bifurcation diagrams, and comparisons with experiments, for the purpose of finding periodic orbits and their stability the stroboscopic sampling method (sampling with the acoustic period) can be more fruitful. This method produces return maps for both phase space coordinates $(R,\ V)$. Figures 8 and 9 show the return maps for R and V respectively at different driving levels. The maps again get very complicated with increasing P_a, but at least there are parameter values where the return map of V is reminiscent of a horseshoe, suggesting that binary symbolic dynamics might suffice to describe the system.

4. Detailed study of the system at chosen parameter values

In this section we find the shortest periodic orbits of the system up to length 5 and their stabilities, which together with the already known cycle periods (an integer times the acoustic period) can be plugged into cycle expansions of trace formulae to compute averages of physical quantities [36]. All the simulations in this chapter used the parameters $P_\text{a} = 1.26\,\text{bar}$, $R_0 = 20\,\mu\text{m}$, $\gamma = 5/3$, and $\omega/2\pi = 27\,\text{kHz}$. At the above parameters the return map of V is a unimodal map, and the value of V where the slope is zero in Figure 9(c) defines the critical point V^*. Introducing the following rules, the system can be described by symbolic dynamics

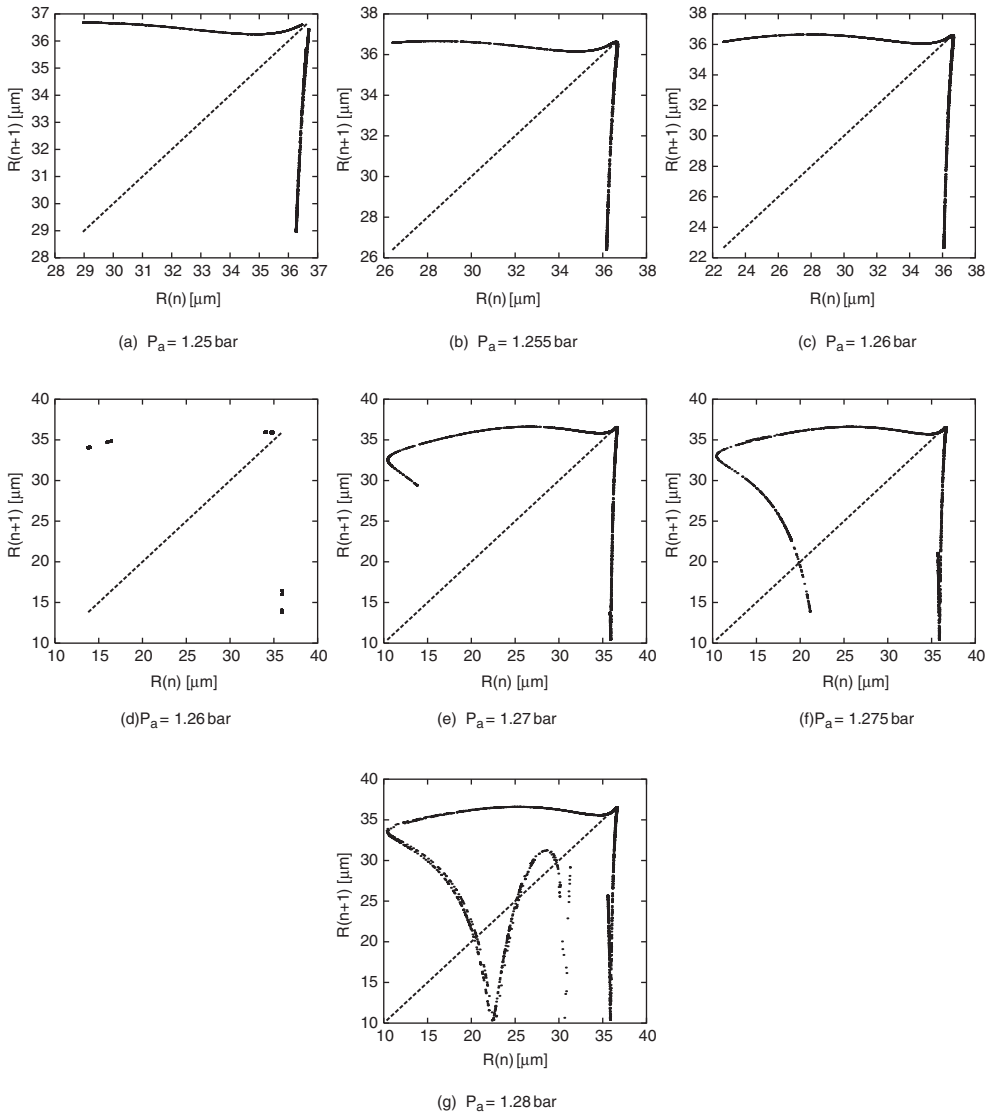

Figure 8. Return maps of bubble radius R, stroboscopically sampled at the end of each period. The other parameters are $R_0 = 20\,\mu\text{m}$, $\gamma = 5/3$, and $\omega/2\pi = 27\,\text{kHz}$.

with a binary alphabet of symbols {0, 1}.

$$V(n) = \begin{cases} 0 & \text{if } V(n) < V^* \text{ (to the left from the critical point),} \\ 1 & \text{if } V(n) > V^* \text{ (to the right from the critical point).} \end{cases} \tag{10}$$

In this notation the itinerary (S^+) of a trajectory starting from the point ζ is given by an infinite sequence of symbols

$$S^+(\zeta) = 10011010001011101000 11\ldots \tag{11}$$

and the itinerary of a prime periodic orbit of length N is labelled

$$S^+(s_1 s_2 s_3 \ldots s_N) = (s_1 s_2 s_3 \ldots s_N)^\infty = \overline{s_1 s_2 s_3 \ldots s_N}, \qquad s_i \in \{0, 1\}. \tag{12}$$

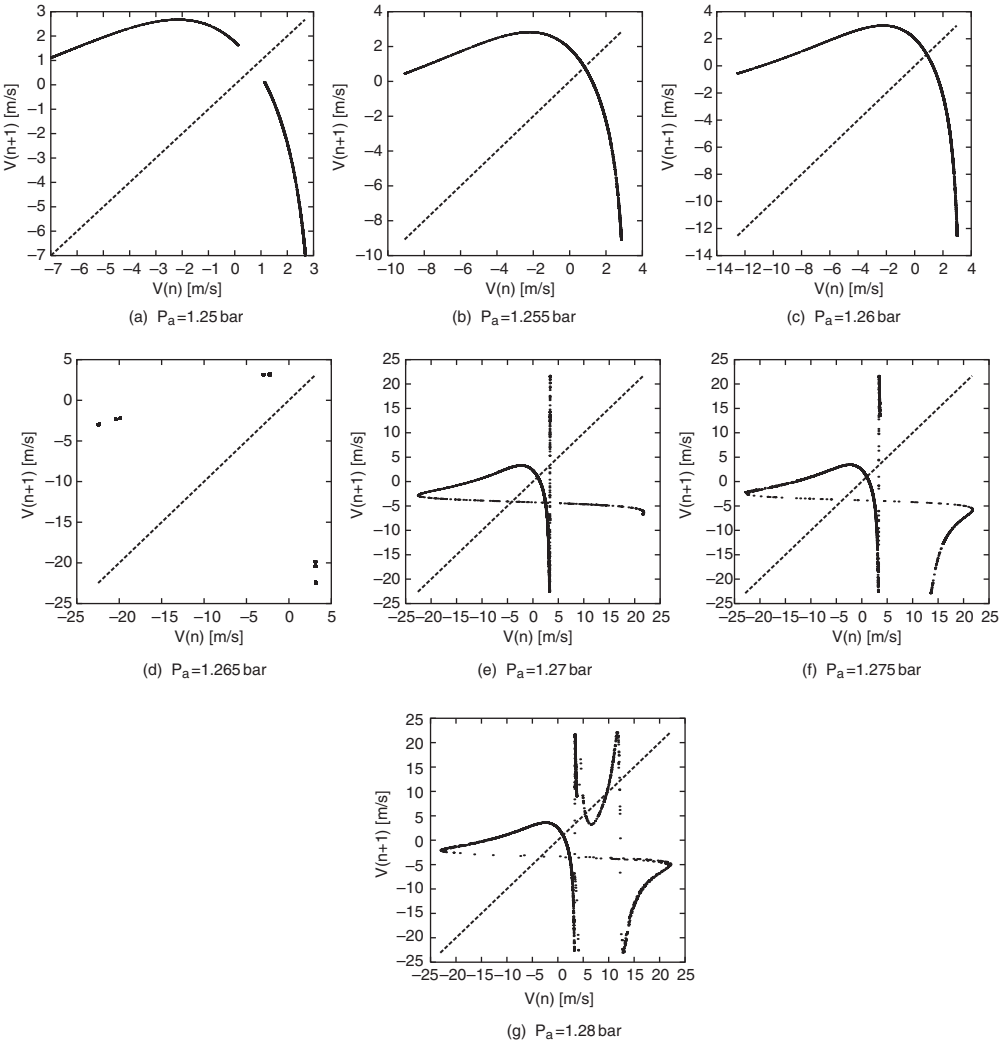

Figure 9. Return maps of the interface velocity V stroboscopically sampled at the end of each period. The other parameters are $R_0 = 20\,\mu\text{m}$, $\gamma = 5/3$, and $\omega/2\pi = 27\,\text{kHz}$.

To find which periodic orbits are realized by the system, one has to generate the list of all admissible itineraries. This can be done to any chosen finite length of the itineraries by applying Kneading's theory (see for instance [37, 38] or Appendix B of [36]). The condition for the admissibility of an itinerary $S^+(s_1 s_2 s_3 \ldots s_N)$ is that its topological coordinate $\gamma(S^+(s_1 s_2 s_3 \ldots s_N))$ should be less than or equal to the topological coordinate of the itinerary corresponding to the critical point $\gamma(S^+(V^*))$:

$$\gamma(S^+(V^*)) \geqslant \gamma(S^+(s_1 s_2 s_3 \ldots s_N)). \tag{13}$$

The itinerary of the critical point is also called the Kneading sequence and its topological coordinate the Kneading value. To generate the topological coordinate of an itinerary it is convenient to replace the binary alphabet $\{0, 1\}$ by the infinite alphabet

$$\{a_1, a_2, a_3, a_4, \ldots; \overline{0}\} = \{1, 10, 100, 1000, \ldots; \overline{0}\}. \tag{14}$$

Table 2. Admissible itineraries and their topological coordinates.

n	Itinerary S	$\gamma(S)$
1	$\overline{1}$	0.10101010101
2	$\overline{10}$	0.11001100110
3	—	—
4	$\overline{1011}$	0.11010010110
5	$\overline{10110}$	0.11011001001
5	$\overline{10111}$	0.11010110101
6	$\overline{101110}$	0.11010011010
6	$\overline{101111}$	0.11010100101

Using this notation the itinerary $S = a_i a_j a_k a_l \ldots$ and its topological coordinate are related by $\gamma(S) = 0.1^i 0^j 1^k 0^l \ldots$. For instance, the Kneading sequence and the Kneading value of this particular system are

$$S^+(V^*) = 10110101011 \ldots = a_2 a_1 a_2 a_2 a_2 a_1 \ldots,$$
$$\gamma(S^+(V^*)) = 0.11011001101 \ldots = 0.1^2 0^1 1^2 0^2 1^2 0^1 1^1 \ldots. \tag{15}$$

For prime periodic orbits the situation is a bit more complicated, because to each of these orbits there will be N itineraries that are cyclic permutations of each other, where N is the period of the orbit. Since all these itineraries will have different values of the topological coordinate, one has to find the maximal among them. Applying criterion (13) one finds for instance that the itineraries $\overline{100}$ and $\overline{101}$ are inadmissible, because both $\gamma(\overline{100}) = 0.111000111000 \ldots$ and $\gamma(\overline{101}) = 0.110110110110 \ldots$ are greater than the Kneading value. Table 2 lists all admissible itineraries of prime periodic orbits up to symbol length 6.

Now that we have found which periodic orbits are realized by the system, the next task is to find their stabilities. The stability of a periodic orbit is given by the eigenvalues of the corresponding d-dimensional Jacobian matrix, which is defined as

$$J^t_{i,j} = \frac{\partial f^t_i(\underline{x}_0)}{\partial x_j}, \qquad i, j \in \{1, \ldots, d\}, \tag{16}$$

where $f^t_i(\underline{x}_0)$ is the ith component of the solution with initial values $\underline{x}_0$, to the differential equations describing the dynamical system $\dot{\underline{x}} = \underline{v}(\underline{x}, t)$ at the time instant t. In our case $d = 2$ and $\dot{\underline{x}} = \underline{v}(\underline{x}, t)$ is represented by equations (3). The elements of the Jacobian can be computed by solving

$$\frac{\mathrm{d}}{\mathrm{d}t} J^t_{i,j} = \sum_{k=1}^{2} A_{i,k}(\underline{x}, t) J^t_{k,j}, \qquad A_{i,k} = \frac{\partial v_i}{\partial x_k}, \tag{17}$$

along the orbit, with initial conditions $J^0_{i,i} = 1$ and $J^0_{i,j} = 0$, where $i \neq j$. The matrix $\underline{\underline{A}}$ is called the derivative matrix, which for the system in hand reads

$$\underline{\underline{A}} = \begin{pmatrix} 0 & 1 \\ a_{21} & a_{22} \end{pmatrix} \tag{18}$$

with

$$a_{21} \equiv \frac{1}{\rho_{\mathrm{w}} R^2}(P_{\mathrm{g}} - P_{\mathrm{f}} - P_0 - P_\eta - P_\sigma + P_{\mathrm{s}}) + \frac{1}{\rho_{\mathrm{w}} R}\left(\frac{4\eta V}{R^2} + \frac{2\sigma}{R^2} - \frac{3\gamma R^2 P_{\mathrm{g}}}{R^3 - a^3} + \frac{P_{\mathrm{a}}}{c}\omega \cos(\omega t)\right)$$

$$-\frac{9\gamma V P_{\mathrm{g}}}{\rho_{\mathrm{w}} c_{\mathrm{w}} R}\left(\frac{R^2(R^3-a^3)-R^5(1+\gamma)}{(R^3-a^3)^2}\right)+\frac{3}{2}\frac{V^2}{R^2}, \tag{19}$$

$$a_{22} \equiv \left(\frac{4\eta}{\rho_{\mathrm{w}} R^2}+\frac{3\gamma R^2 P_{\mathrm{g}}}{\rho_{\mathrm{w}} c_{\mathrm{w}}(R^3-a^3)}+\frac{3V}{R}\right). \tag{20}$$

The expressions of the pressure terms P_{g}, P_{f}, P_η, P_σ and P_{s}, as a function of the phase space coordinates and time, are already given in equations (2) and (4). An efficient way to find periodic orbits is to use the Newton method sketched below. One starts with an initial guess $\underline{x}$ for the location of a fixed point in the Poincaré section, which is in our case $\underline{x} = (R, V)$ at time zero. Then one has to evolve the initial point, together with the Jacobian, and find their values $f(\underline{x})$ and $\underline{\underline{J}}$ after an acoustic period. Inserting these into

$$\underline{x}' = \underline{x} - (1 - \underline{\underline{J}})^{-1}(\underline{x} - f(\underline{x})) \tag{21}$$

yields the improved guess $\underline{x}'$. Iterating the routine, the guesses converge faster than exponentially to the right values. In practice this means that, for instance, if one wishes to know the coordinates of a fixed point accurate to ten digits, then it requires around 5–7 iterations, even if the initial guesses are quite rough. A problem can arise if the Jacobian has an eigenvalue 1 for some reason, because in that case the matrix $(1 - \underline{\underline{J}})$ is not invertible. There are techniques to overcome such difficulties (see chapter 9 of [36]), but fortunately in our case we do not have to deal with this problem.

Good starting values can be obtained from n-return maps of the phase space coordinate V, because a prime orbit of length n will show up as n identical fixed points in such maps (see figure 10). Table 3 lists the prime cycles up to length 5, their stability eigenvalues, periods, Liapunov exponents, and the coordinates of the fixed point, where the Newton iteration converged. A part of the orbits is shown in figure 11.

The information contained in the stability and period of prime periodic orbits can be used to calculate global properties, such as the Liapunov exponent, or averages of physical quantities of interest for the particular system. For instance, in our case this quantity can be the concentration of the gas in the liquid C_i, at which the bubble is in diffusive equilibrium with the surroundings. For stable periodic oscillations this is given by

$$C_i = C_0 \frac{\int_0^T R(t)^4 P_{\mathrm{g}}(R(t))\,\mathrm{d}t}{P_0 \int_0^T R(t)^4\,\mathrm{d}t}, \tag{22}$$

where C_0 is the constant equilibrium air concentration at an ambient pressure of 1 bar, and the integration is done over one acoustic period (see e.g. [39–43]). If the oscillations are chaotic, one has to do the above integrals over a very long time, until the trajectory covers the whole attractor (figure 4). According to [36] the average over the covered part of the phase space can be rewritten as an average over the unstable periodic orbits.

Before proceeding any further, it is worth noting that the system satisfies the hyperbolicity assumption (at least in the case of the few studied orbits), which is a requisite to apply the forthcoming methods. Skipping a lot of details and considerations (which can be found in [36]), here we just state that for a bound system with zero escape rate the phase space average of a time-integrated quantity A can be expressed through an infinite sum over the properties of the prime periodic orbits,

$$\langle A \rangle = \sum_{\{p_1, p_2 \cdots p_k\}}{}' (-1)^{k+1} \frac{A_{p_1} + A_{p_2} + \cdots + A_{p_k}}{|\Lambda_{p_1} \Lambda_{p_2} \cdots \Lambda_{p_k}|}, \tag{23}$$

where the sum is taken over all distinct non-repeating combinations of prime cycles with topological length k ($k = 1 \ldots \infty$), Λ_{pk} is the expanding eigenvalue of the Jacobian evaluated

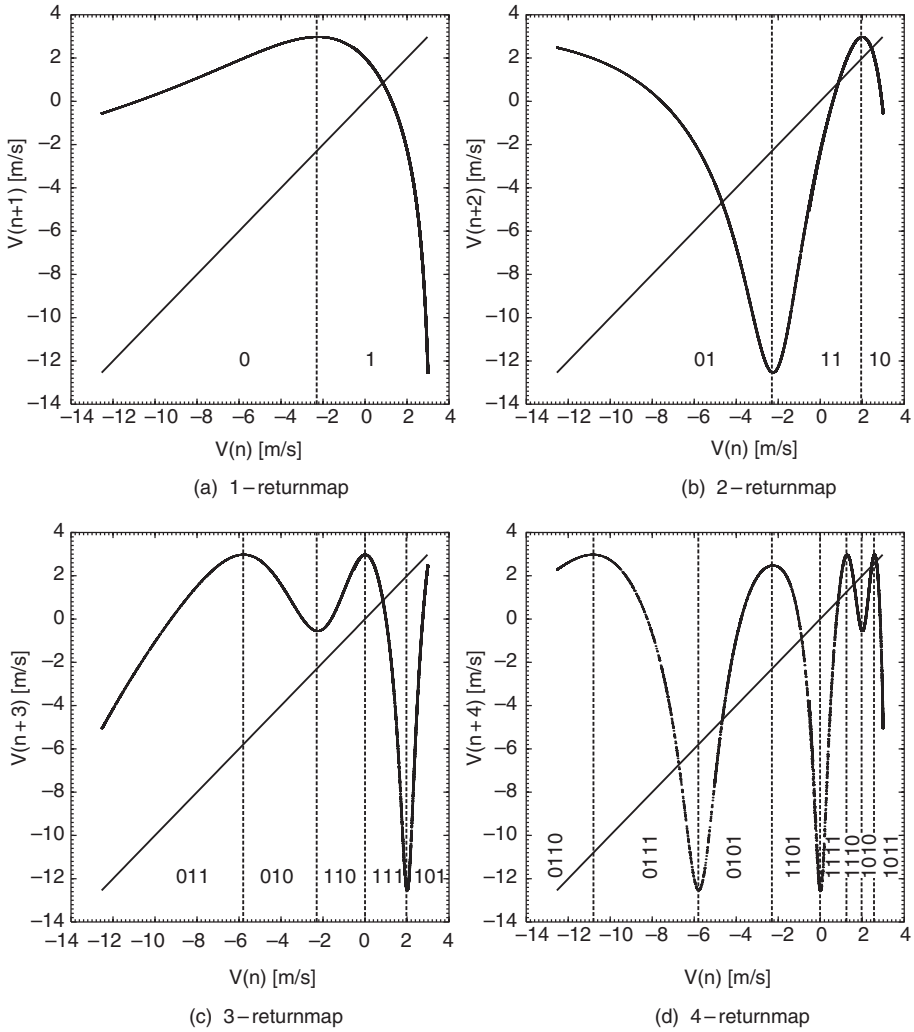

Figure 10. N-return maps of V. The vertical lines separate spatial regions with different itineraries. For instance, if a trajectory is started from a region marked 010 it means that initially it was on the left of the 1-return map, in the next step it will be on the right side, and finally it will end up on the left.

Table 3. Stable and unstable eigenvalues of the Jacobian, Liapunov exponents, and the coordinates of the fixed points for the first five prime periodic orbits.

n	Itinerary	Λ_s	Λ_u	$\lambda = \ln(\lvert\Lambda_u\rvert)/T\,(s^{-1})$	$R(\mu m)$	$V\,(m\,s^{-1})$
1	$\overline{1}$	−0.003 002 373	−1.752 777 328	15152.4	36.585 942 554	0.830 082 401
2	$\overline{10}$	$-1.659\,79 \times 10^{-5}$	−2.757 133 837	13691.5	36.351 426 255	2.423 921 084
3	—	—	—	—	—	—
4	$\overline{1011}$	-2.4×10^{-10}	−7.148 450 714	13276.5	36.226 011 047	2.654 682 468
5	$\overline{10111}$	1.9×10^{-12}	7.393 516 311	10803.3	36.100 765 029	2.889 400 458
5	$\overline{10110}$	-2.6×10^{-12}	−6.078 932 905	9746.1	36.084 527 077	2.926 305 255

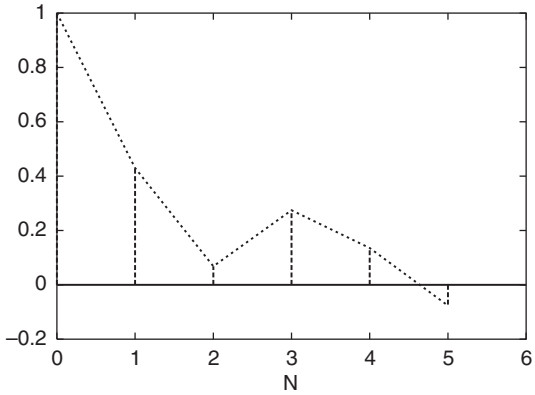

Figure 11. The convergence of escape rate to zero, with increasing topological length of truncation.

along the orbit, and A_{pk} denotes that the physical quantity is integrated in time over the orbit period T_{pk} (the orbit period is an integer times the acoustic period in our case). In practice one always uses a truncated version of the above formula, but that still gives good approximations, since the contribution of cycles diminishes with their topological length. For convenience the truncated (at topological length 5) version of equation (23) applied for the system at hand is shown below:

$$\langle A\rangle = \frac{A_{p_1}}{\left|\Lambda_{p_1}\right|} + \frac{A_{p_{10}}}{\left|\Lambda_{p_{10}}\right|} + \frac{A_{p_{1011}}}{\left|\Lambda_{p_{1011}}\right|} + \frac{A_{p_{10111}}}{\left|\Lambda_{p_{10111}}\right|} + \frac{A_{p_{10110}}}{\left|\Lambda_{p_{10110}}\right|} - \frac{A_{p_1}+A_{p_{10}}}{\left|\Lambda_{p_1}\Lambda_{p_{10}}\right|} - \frac{A_{p_1}+A_{p_{1011}}}{\left|\Lambda_{p_1}\Lambda_{p_{1011}}\right|}. \quad (24)$$

The validity of the approximation can be checked by flow conservation sum rules such as

$$0 = 1 - \sum_{\{p_1,p_2\cdots p_k\}}{}' (-1)^{k+1}\frac{1}{\left|\Lambda_{p_1}\Lambda_{p_2}\cdots\Lambda_{p_k}\right|}, \quad (25)$$

which is exact if the sum involves infinite cycles. This formula gives the escape rate of trajectories, which for a bounded system equals zero. Figure 12 shows to what degree equation (25) is satisfied as a function of the truncation. The non-monotonic and relatively slow convergence can be attributed to the effect of pruning, since in this case there is only partial shadowing. For instance, there is no 101-term present which would almost cancel the contribution of the $1\cdot 10$-term; thus there is a hump in figure 11 at $N = 3$.

5. Averages of physical quantities

This section gives the results of applying the method discussed in the previous section for the dimensionless equilibrium concentration C_i/C_0. Water under normal conditions contains an amount of dissolved air with concentration C_0. In experiments one usually sets C_i to be a fraction of the normal value to achieve equilibrium, otherwise the bubble would grow from cycle to cycle by rectified diffusion [39–43]. It is worth mentioning that in the applications the acoustic period is much smaller than the timescale of diffusion. If this would not hold, one would have to use a modified RP equation which incorporates diffusion. For convenience, equation (22) is rewritten as

$$\frac{C_i}{C_0} = \frac{A_p}{B_p}, \qquad A_p = \int_0^{T_p} R(t)^4 P_{\mathrm{g}}(R(t))\,\mathrm{d}t, \qquad B_p = P_0\int_0^{T_p} R(t)^4\,\mathrm{d}t. \quad (26)$$

Table 4 contains the values of A_p and B_p obtained for the shortest cycles.

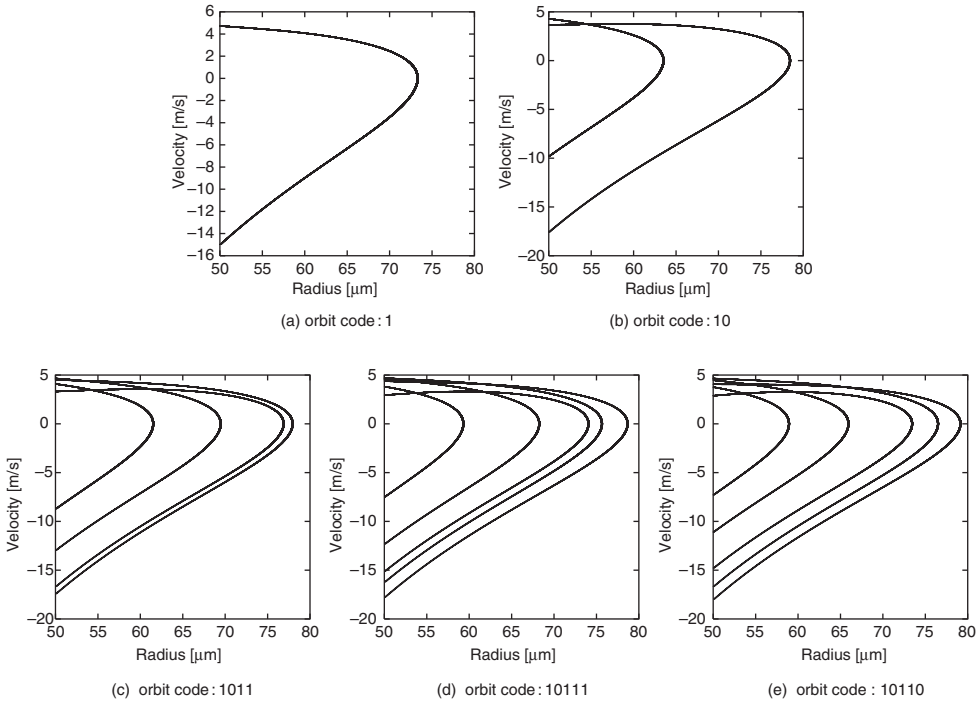

Figure 12. Prime periodic orbits up to a topological length of 5 symbols. The pictures show a blowup of the phase space near the maximal radii.

Table 4. The values A_p and B_p integrated along the calculated prime orbits.

n	Itinerary	A_p	B_p
1	$\overline{1}$	$3.658\,410\,33 \times 10^{-24}$	$2.770\,306\,05 \times 10^{-22}$
2	$\overline{10}$	$7.345\,372\,47 \times 10^{-24}$	$5.442\,509\,36 \times 10^{-22}$
3	—	—	—
4	$\overline{1011}$	$1.468\,173\,06 \times 10^{-23}$	$1.086\,670\,31 \times 10^{-21}$
5	$\overline{10111}$	$1.836\,756\,29 \times 10^{-23}$	$1.342\,018\,73 \times 10^{-21}$
5	$\overline{10110}$	$1.838\,085\,64 \times 10^{-23}$	$1.335\,144\,17 \times 10^{-21}$

Using the data of table 4 and equation (24), the result for the equilibrium concentration is

$$\frac{C_i}{C_0} = \langle A \rangle / \langle B \rangle = 0.013\,608. \tag{27}$$

This means that in order to be in diffusive equilibrium with the surrounding liquid, the water has to be de-gassed to 1.36% of its concentration at normal conditions. For stable oscillations it is customary (and satisfactory) to calculate the above integrals only for one acoustic cycle, and with initial values $R(t = 0) = R_0$, $V(t = 0) = 0$. The question can arise as to how big an error will one get by applying these rules for the chaotic case. The calculation for C_i/C_0 in this case gives 0.0301, showing a considerable difference. This can be improved if one integrates for many acoustic cycles. In figure 13 the (+) symbols show the calculations over N acoustic periods, with initial conditions $R(t = 0) = R_0$, $V(t = 0) = 0$. The other symbols ($\times$) indicate the convergence of C_i/C_0 as the topological length of the truncation is increased in equation (24). It is apparent from the figure that after 50 acoustic periods the two methods

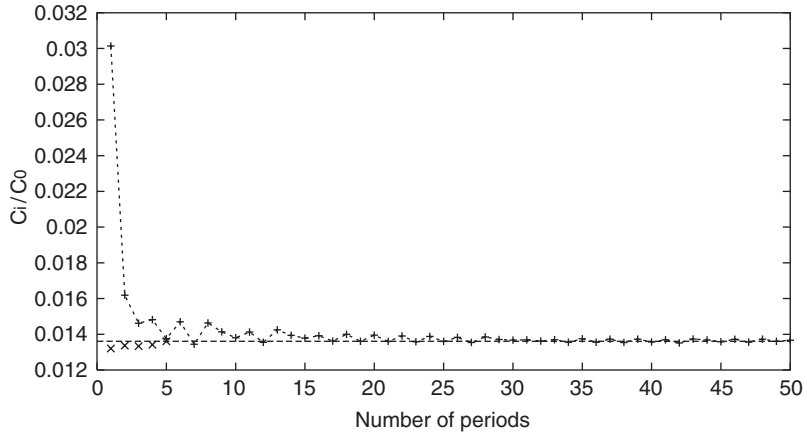

Figure 13. Convergence of the physical quantity $C_i = C_0$. Symbols (+) were obtained by integrating over N periods, and using the initial conditions $R(t = 0) = R_0$, $V(t = 0) = 0$, while the symbols ($\times$) denote the cycle expansions for the first N orbits. The horizontal line shows the value obtained by 5 prime cycles.

give identical results, and that for a good approximation it was enough to consider prime cycles up to topological length 5 in the cycle-expansion formula (24). One can also check how good an approximation can be obtained by considering only the first prime periodic orbit. In this case one gets $C_i/C_0 = 0.0132$, a value fairly close to that obtained with five prime cycles. Even though the two methods agree in this particular example, it cannot be guaranteed in general that for a quantity which depends differently on R and V, integration over 50 periods will be sufficient to achieve convergence. Thus if possible it is always better to apply periodic orbit theory and use cycle-expansion formulae to calculate the physical quantities of a chaotic system, because the results obtained by this technique converge faster with the topological length. Another advantage of the method is that once the properties of the prime periodic orbits are known (period, stability eigenvalue, and the coordinates of the fixed points), they are readily available for the calculation of other physical quantities. Thus for each new quantity one has to integrate only over a few prime cycles, instead of many periods until achieving a steady value.

6. Conclusion

The RP dynamics of a driven gas bubble has been investigated in the stable and chaotic regimes. Concerning period doubling and chaos, the same qualitative behaviour was observed as in the previous paper by Lauterborn and Suchla [13] who studied a slightly different bubble dynamical model and considered much bigger bubbles ($R_0 \geqslant 100\,\mu$m). By scanning a large parameter space, all the transients are found to die out in less than ten cycles for $R_0 \leqslant 6\,\mu$m, which implies that at the studied acoustic frequency the solutions to the RP equation are stable in the whole parameter space of SBSL. This provides strong evidence for the assumption that radial RP dynamics is insufficient to explain the period-doubling, quasiperiodic and chaotic behaviour observed in the measurements of Holt *et al* [11] and Jensen [12]. By constructing return maps we showed that at particular values of the parameter P_a the return map is unimodal; thus binary symbolic dynamics can be used to describe the system. The list of admissible prime cycles up to symbol length 6 is found by applying Kneading's theory. The information contained

in the stability and periods of the first few prime cycles can be used to calculate averages of physical quantities relevant for the system. We show this on a particular example and find that the time-averaged value of this quantity converges to the value obtained from the truncated cycle expansion formula.

Acknowledgments

The authors acknowledge financial support from the Danish Nonlinear School and the Hungarian National Research Foundation OTKA under grant F025840. GS also wishes to thank Per Dahlqvist, Peter S Jensen, and Rytis Pakauskas for ecouragement, suggestions and valuable discussion, and the hospitability of the CATS group at the Niels Bohr Institute.

References

[1] Gaitan D F, Crum L A, Roy R A and Church C C 1992 *J. Acoust. Soc. Am* **91** 3166
[2] Gaitan D F 1990 *PhD thesis* University of Mississippi
[3] Barber B P *et al* 1997 *Phys. Rep.* **281** 65
[4] Barber B P and Putterman S J 1991 *Nature* **352** 318
[5] Gompf B, Günther R, Nick G, Pecha R and Eisenmenger W 1997 *Phys. Rev. Lett.* **79** 1405
[6] Pecha R, Gompf G, Nick G, Wang Z Q and Eisenmenger W 1998 *Phys. Rev. Lett.* **81** 717
[7] Moran M J and Sweider D 1998 *Phys. Rev. Lett.* **80** 4987
[8] Hiller R A, Putterman S J and Barber B P 1992 *Phys. Rev. Lett.* **69** 1182
[9] Hiller R A, Putterman S J and Weninger K R 1998 *Phys. Rev. Lett.* **80** 1090
[10] Barber B P, Hiller R A, Arisaka K, Fetterman H and Putterman S J 1992 *J. Acoust. Soc. Am.* **91** 3061
[11] Holt R G, Gaitan D F and Atchley A A 1994 *Phys. Rev. Lett.* **72** 1376
[12] Jensen P S 1998 *MSc Thesis* Niels Bohr Institute/CATS
[13] Lauterborn W and Suchla E 1984 *Phys. Rev. Lett.* **53** 2304
[14] Lauterborn W and Koch A 1987 *Phys. Rev.* A **35** 1974
[15] Smereka P, Birnir B and Banerjee S 1987 *Phys. Fluids* **30** 3342
[16] Holzfuss J and Lauterborn W 1989 *Phys. Rev.* A **39** 2146
[17] Parlitz U, Englisch V, Scheffczyk C and Lauterborn W 1990 *J. Acoust. Soc. Am.* **88** 1061
[18] Rayleigh L 1917 *Phil. Mag.* **34** 94
[19] Plesset M 1949 *J. Appl. Mech.* **16** 277
[20] Löfstedt R, Barber B P and Putterman S J 1993 *Phys. Fluids* A **5** 2911
[21] Prosperetti A 1977 *J. Acoust. Soc. Am.* **61** 17
[22] Press W H, Teukolsky S A, Vetterling W T and Flannery B P 1992 *Numerical Recipes in C* (Cambridge: Cambridge University Press)
[23] Prosperetti A 1977 *Q. Appl. Math.* **34** 339
[24] Brenner M P, Lohse D and Dupont T F 1995 *Phys. Rev. Lett.* **75** 954
[25] Hilgenfeldt S, Lohse D and Brenner M P 1996 *Phys. Fluids* **8** 2808
[26] Wu C C and Roberts P H 1998 *Phys. Lett.* A **250** 131
[27] Prosperetti A and Hao Y 1999 *Phil. Trans. R. Soc.* A **357** 203
[28] Augsdörfer U H, Evans A K and Oxley D P 2000 *Phys. Rev.* E **61** 5278
[29] Weninger K R, Camara C G and Putterman S J 2001 *Phys. Rev.* E **63** 016310
[30] Matula T J, Hallaj I M, Cleveland R O and Crum L A 1997 *J. Acoust.Soc. Am.* **103** 1377
[31] Holzfuss J, Rüggeberg M and Billo A 1998 *Phys. Rev. Lett.* **81** 5434
[32] Pecha R and Gompf B 2000 *Phys. Rev. Lett.* **84** 1328
[33] Barber B P and Putterman S J 1992 *Phys. Rev. Lett.* **69** 3839
[34] Holt R G and Crum L A 1992 *J. Acoust. Soc. Am.* **91** 1924
[35] Simon G, Csabai I, Horváth Á and Szalai F 2001 *Phys. Rev.* E **63** 026301
[36] Cvitanović P, Artuso R, Mainieri R and Vattay G 2000 *Classical and Quantum Chaos* `www.nbi.dk/ChaosBook/`, Niels Bohr Institute (Copenhagen)
[37] Katok A and Hasselblatt B 1995 *Introduction to the Modern Theory of Dynamical Systems* (Cambridge: Cambridge University Press)

[38] Hao Bai-lin 1989 *Elementary Symbolic Dynamics and Chaos in Dissipative Systems* (Singapore: World Scientific)
[39] Eller A and Flynn H G 1965 *J. Acoust. Soc. Am.* **37** 493
[40] Fyrillas M M and Szeri A J 1994 *J. Fluid Mech.* **277** 381
[41] Löfstedt R, Weninger K R, Putterman S J and Barber B P 1995 *Phys. Rev.* E **51** 4400
[42] Brenner M P, Lohse D, Oxtoby D and Dupont T F 1996 *Phys. Rev. Lett.* **76** 1158
[43] Roberts P H and Wu C C 1998 *J. Theoret. Comput. Fluid Dynamics* **10** 357